26 Nondestructive testing of repair mortars for concrete

C. Jaquerod, Alusuisse Aluminium Suisse s.a. - Division laminoirs -
CH Chippis, F. Alou and Y.F. Houst, Ecole Polytechnique Fédérale - Lab. matér. de construction - CH Lausanne

Abstract

The concrete structures of Swiss highways are subject to severe conditions. To reduce repair cost it is necessary to detect on time the various degradations. These reasons have led us to conceive a repair mortar for concrete structures. In association with the commonly used test methods for mortar, we have evaluated the mortar quality by ultrasonic pulse velocity measurements.
A good correlation between compressive strength and ultrasonic pulse volocity, both measured on cast specimens, has been found. This same method, applied to in situ mortar, allowed us to evaluate the quality of the substrate and the presence of cracks, even when they are non-apparent. Simulation has shown that tensile stresses higher than the intrinsic strength of the material can appear in the neighbourhood of the concrete-mortar interface, depending on drying conditions. Therefore, the risk of cracking is high and that is why the cure of the mortar is particulary important. Mechanical properties of this mortar are comparable to those of current concrete. A limited shrinkage combined with a high creep reduces the risk of cracking when the curing conditions are good enough.

1 Introduction

The Swiss national network of highways has 2900 bridges, with a replacement value of 5 billions Swiss francs. According to date of construction, the annual cost for maintenance and inspection varies from 1.5% to 3% of the capital cost of the structure. These constatations have led the National Office for Highways (OFR) to encourage a systematic research about the maintenance of bridges, the highlight being:

- evaluating the state of the structure
- developing and evaluating new materials
- choosing new methods of repairing

In this context we propose a repair mortar, whose quality is determined by ultrasonic testing. The study is completed by a numerical simulation about the risk of cracking or decohesion of the mortar/concrete interface.
Repair mortars must in the first place be insensitive to the atmospheric conditions. Due to the varying quality of the substrate, adhesion is also a very important parameter. The elastic modulus and compressive strength of the mortar should be equivalent to those of concrete, in order to avoid discontinuites in the stresses due to the static conditions of the structure. Finally, an elevated creep strength limits the risk of cracking. It has nevertheless of be combined with a low shrinkage and a thermal expansion as near as possible to that of concrete. The last parameters to specify are alkalinity and permeability: the latter should be low in order to limit diffusion of carbon dioxide or chlorine ions. A low permeability combined with a high alkalinity allows to keep the reinforcing bars of the structure in an inert electrochemical state, which guarantees their dimensional stability.
In order to satisfy these various demands it is possible to use synthetic- or hydraulic-base mortars. We have limited ourselves to hydraulic mortars, essentially for cost reasons. These mortars contain condensed silica fume, associated with a superplasticizer admixture. This solution contains many advantages, particularly for durability. Resistance to freeze-thaw cycles and deicing salts are improved, whereas permeability and diffusion of chlorine ions are reduced, without decreasing the mechanical properties of the mortar.

2 Experimental

2.1 Materials

The Portland cement from the plant at Eclépens (Switzerland), was approximately of ASTM type I, with fineness defined by specific area 290 m^2/kg (Blaine). The condensed silica fume (CSF) was imported form Germany (trademark: V.A.W. RW Füller) in a grey powder slightly densified. The silica content was 96.5% of amorphous silica, the BET specific surface area was 20'000 to 22'000 m^2/kg, and the specific gravity 2'200 kg/m^3.,
The sand (0-4 mm) was from a glacial moraine of rounded shape. Mineralogically, the sand was composed of 40 to 46 % calcite, 29 to 32% quartz, 8 to 13% residue of crystalline rocks of multimineral composition, predominantly quartzitic, and 12 to 18% of composite grains, essentially quartzitic.

For all the tests only one superplasticizer, consisting of sulfonated melamine formaldehyde condensate, has been used. The dosage of this admixture was 2% by mass of the cement. It was added after the water.
For this study, three mortars have been used. Their composition is given in table 1. All have the same cement/sand ratio 1/3, 10% of CSF and 2% of superplasticizer relative to the mass of cement. The compostion was chosen on the basis of preliminary tests. The mortars differ only from one another in water/cement ratio.

Table 1: Composition of the Mortars

Mortar No	1		2		3	
	kg/m^3	L/m^3	kg/m^3	L/m^3	kg/m^3	L/m^3
Cement	507	163	500	161	495	160
Silica fume	50	20	50	19	49	19
Superplasticizer	10	8	10	8	10	8
Water	203	203	210	210	223	223
Sand	1520	569	1500	562	1485	556
Air	--	38	--	40	--	35
Total	2290	1000	2270	1000	2260	1000
Water/Cement	0.40		0.42		0.45	

Normalized prisms 40/40/160 mm, with a water/cement ratio varying between 0.35 and 0.50, have been specially prepared to measure compressive strength and ultrasonic pulse velocity at 7 and 28 days.

2.2 Testing methods

Flexural and compressive tests have been carried out on conventional prisms 40/40/160 mm used for normalized tests on cement. After the flexural test, the two parts of the specimen were used for the compressive test. The prisms have been kept up to the day of the test at a relative humidity > 95% at 20 ± 1°C.
The elastic modulus was measured on prisms 40/40/160 mm after 28 days of curing in the same conditions as cited before, in accordance with Swiss standard SIA 162/1.
For shrinkage measurements, the specimens (prisms (60/60/320) were cured at a relative humidity > 95% and at 20 ± 1°C, until their exposure to the drying environment. This type of curing is preferable to curing in a water bath,

which has been found to cause nonuniform water intake, significant swelling stresses, and microcracking. The environmental humidity was 60 ± 5% and the room temperature was 20 ± 1°C throughout the shrinkage.
The shrinkage deformations were measured by taking length readings between the ends of the specimens along the prism axis. The deformations of all specimens were measured with one dial gauge which had contact made of steel balls that fit into ringshaped steel targets attached before the molds were stripped. All the specimens were exposed to drying after 14 days and shrinkage measurements started immediately. The initial reading, representing the zero strain, was taken within 1 minute after placing of the specimen in its set-up; in previous tests the first reading was apparently taken much later, causing a significant initial shrinkage to go unrecorded.
The creep measurements were carried out on specimens of the same section as those for shrinkage measurements but with a height of 250 mm. The specimens were cured under the same conditions and with the same caution. Then, they were placed at the age of 14 days into their set-up. The stress was maintained at ± 5% by a gas pressure accumulator. The mean applied stress was 7 MPa.
The adhesive tensile strength was measured by the pull-off test on cores (diameter 74 mm) drilled through the repair mortar and within the concrete substrate. Two metal discs were glued in the end surfaces of the cores by means of an epoxy adhesive. The force necessary to pull off the glued core was measured with a tension test machine. Two types of specimens can be distinguished:

- for type 1, half-cubes of concrete (200/200/200 mm), obtained by the "Brazilian test" were used. The mortars were applied horizontally by means of a trowel. The specimens were kept at the climatic laboratory conditions, i.e. 60 ± 10% RH and 20 ± 2°C.
- for type 2, the repair mortar was applied vertically on a concrete wall with aggregates partially exposed by two masons by means of a trowel. The mortar was nº3 (W/C = 0.45), but the masons could add water to it, the amount being measured, until it obtained the desired consistency. To obtain a thickness of 50 mm, it was necessary to apply 3 layers. The first was 10 mm thick, the second 25 mm and the last one 15 mm. 24 hours had elapsed between applications. The mortar was applied outdoors on the two faces of the wall, facing North-East (without solar radiation) and South-West (with solar radiation). Between the parts applied by the masons, repair mortar was applied horizontally, as for a screed. The climatic conditions during the application of the mortar were 20 to 23°C and 63 to 71% relative humidity. The water/cement ratio of the different layers of mortar depending on the mason are given in table 2.

Table 2: W/C ratios used by the masons during the manual application of the mortar

Layer No	mason A	mason B
1	0,57	0,62
2	0,56	0,55
3	0,56	0,54

2.3 Analysis of the velocity of sound in an homogeneous and isotropic material

The propagation of sonic waves in a material assumed to be homogeneous and isotropic is described by the following equations:

$$\mathrm{div}\sigma - \rho \frac{\partial^2 \vec{u}}{\partial t^2} = 0 \qquad (1)$$

$$\sigma = S\,\varepsilon \qquad (2)$$

Where:
- σ is the stress tensor
- ε is the strain tensor
- S is the elastic constants tensor
- u is the displacement vector of the wave

$$\varepsilon = \frac{1}{2}(\mathrm{grad}\vec{} + \mathrm{grad}\vec{}^{T})\vec{u} \qquad (3)$$

The plane waves (4) solutions of the previous expressions are of 3 types, namely:
- longitudinal or compressive waves
- transverse or shear waves
- Rayleigh's or surface waves

$$\vec{u} = \vec{u}_0 \exp[i(\omega t - \vec{k}\vec{r})] \qquad (4)$$

The velocity of these waves depends on the density and elastic constants of the material, according to the following relations:

$$v_L^2 = \frac{E}{\rho}\frac{(1-\nu)}{(1+\nu)(1-2\nu)} \quad \text{compressive waves} \qquad (5)$$

$$v_T^2 = \frac{E}{\rho}\frac{1}{2(1+\nu)} \quad \text{shear waves} \qquad (6)$$

$$v_S^2 = v_L^2 + v_T^2 \quad \text{surface waves} \qquad (7)$$

Two modes of measurements are used for this study, shown on figure 1; the direct mode is used for the calibrations on normalized prisms, whereas the indirect mode is used for in situ testing. Though the piezoelectric captor is polarized for a compressive excitation, the scattering of the sonic impulses by the mortar requires that the measurements be calibrated. Those tests have shown that the velocity of sound does not depend on the water content in the mortar. We assume the following equality between the velocities determined by the indirect and the direct mode:

$$f_{di} = \frac{\text{velocity}_{\text{direct measurement}}}{\text{velocity}_{\text{indirect measurement}}} = 104 \pm 0.01 \qquad (8)$$

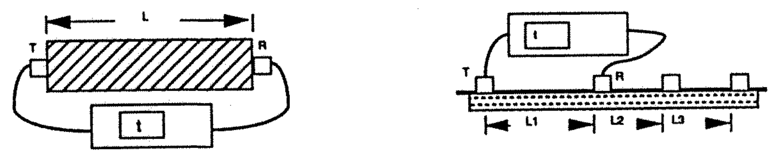

T: emitting transducer — excitation frequency 50 kHz
R: receiving transducer — frequency band 2 - 200 kHz
t: measured passing time through the sample for the acoustic pulse

Figure 1: Principle schemes of measurements; direct mode (left), indirect mode (right). The acoustic coupling between the captors and the material is provided by a layer of bentonite gel.

2.4 Numerical simulation

The following modelling has been realised with the help from Dr. Pieter Roelfstra, INTRON CSME BV, CH - 1400 Yverdon-les-Bains.

2.4.1 *Evolution of the relative humidity in a wall during curing*

Nomenclature

λ	: permeability	[kg/ms]
C	: water-holding capacity	[kg/m^3]
H	: relative humidity	[%]
t	: time	[s]
x	: position	[m]

The mesh used for this computation is shown on figure 2. The equation to solve is the diffusion equation (9).

$$\text{div}\,\lambda\,\overrightarrow{\text{grad}}H = C\frac{\partial H}{\partial t} \qquad (9)$$

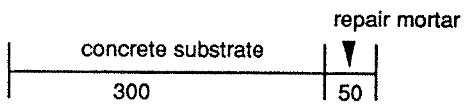

Figure 2: One-dimensional mesh used for computing the relative humidity with time

The water-holding capacities are extracted from literature [1,2]. The permeability is calculated from the following relation and with the help of Bazant and Najjar's model [3], which describes the dependence of the coefficient of diffusion on the relative humidity. For the computation the initial and boundary conditions were as follows:

– initial humidity in mortar	100%
– initial humidity in concrete	60%
– temperature in the mortar	18°C
– external humidity	60%

2.4.2 *Development of stresses and strains in a wall during curing*

Nomenclature

ε	: deformation	[–]
σ	: stress	[MPa]
E	: elastic modulus	[GPa]
t	: time	[s]
τ_i	: characteristic time for Maxwell's i^{th} element	[s]
p_i	: power exponent for Maxwell's i^{th} element	[–]

The mesh used here is similar to that used before, with a height of 2000mm. The development of stresses in a wall is described by the equation (10), the term D_{ijkl} taking the effects due to creep into account.

$$\sigma_{ij} = D_{ijkl}\left[\varepsilon_{tot} - \varepsilon_{shrinkage} - \varepsilon_{therm}\right] \qquad (10)$$

The viscoelastic deformation of the materials is fitted to a generalized Maxwell's element with 6 components, each of these having

$$\varepsilon_m = \frac{\sigma}{E_m}\left[1+\left(\frac{t}{\tau_m}\right)^{p_m}\right] \qquad (11)$$

The parameters E_m, τ_m and p_m have been obtained on the basis of experiments performed in the laboratory. The deformation due to shrinkage is fitted from experimental results, whereas the one due to thermal dilatation is computed from a thermodynamical model presented by Roelfstra [4].
With a piecewise linear assumption for the global behaviour of the materials, one obtains the following incremental equations for the development of stresses:

$$\Delta\sigma_{ij} = \sum_{m=1}^{n}\left[1-e^{\frac{\Delta t}{\tau_m}}\right]\left[D'_{ijkl}E_m\frac{\tau_m}{\Delta t}\Delta\varepsilon_{kl} - \sigma_{ij}^{t-\Delta t}\right] \qquad (12)$$

$$\sigma_{ij}^{t} = \sigma_{ij}^{t-\Delta t} + \Delta\sigma_{ij} \qquad (13)$$

$$D'_{ijkl} = \frac{1}{2(1+\nu)}\left[\frac{2}{(1-2\nu)}\delta_{ij}\delta_{kl} + \delta_{ik}\delta_{jl} + \delta_{il}\delta_{jk}\right] \qquad (14)$$

Finally, we have assumed plane strain conditions for all computations, which means $\varepsilon_{13} = \varepsilon_{23} = \varepsilon_{33} = 0$

3 Results

3.1 Mechanical testing

Whereas flexural strength of these mortars remains equal to those for standard mortars, compressive strengths are high, due to the reduction of the size of the transition zone surrounding the aggegates by the pouzolanic reactions. Similar tests performed on standard prisms have shown that W/C ratio is the determining parameter to obtain high strengths. In practice these

strengths will be lower because of the W/C that can be higher and the curing less favorable.
The British standard BS8110:part2:1985 permits to relate static and dynamic modulus of elasticity, with

$$E_{stat} = 1.25\, E_{dyn} - 19$$

The results of shrinkage tests are given in figure 3. The values obtained for the mortars hardly differ but the shrinkage does vary with the water/(cement + CSF) ratio. Using the mean values of the three mortars and the following equation:

$$\varepsilon = a\sqrt{\frac{t}{b+t}} \qquad (15)$$

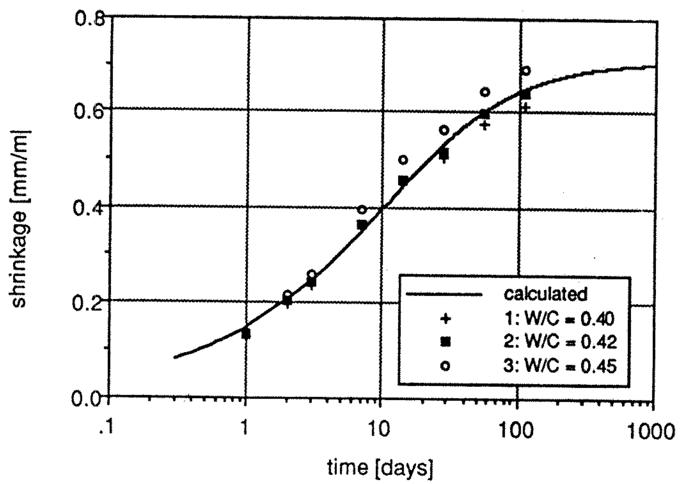

Figure 3: shrinkage of the mortars

which describes the shrinkage as a function of time [5], we can determine the parameters a and b by the least squares method. We obtain:

$$a = 0{,}71 \text{ mm/m} \qquad b = 22 \text{ days} \qquad (16)$$

The value of the final shrinkage (a) is low if one takes into consideration the relative humidity and the specimen size. For concrete, a value of 0.76 mm/m can be expected [6].
The measurements of creep strains as a function of time on specimens under a stress of 7 MPa are given in Figure 4. It can be seen that the strains are practically independent of the W/C ratio. The creep value after 112 days is about two times the elastic strain. The creep strains for our mortars are higher than those of good concrete. This naturally limits cracking.
The results of the adhesive tensile strength are given in tables 3 and 4. It can be seen that, in two cases, adhesive strength increases with time, even for the specimens exposed outdoors. The results after 56 days represent between 75% (type 1) and 80% (type 2) of the tensile strength of the concrete. No crack could be observed on a wall of 2 x 1m^2. The fracture surface showed always at least 25% of concrete.

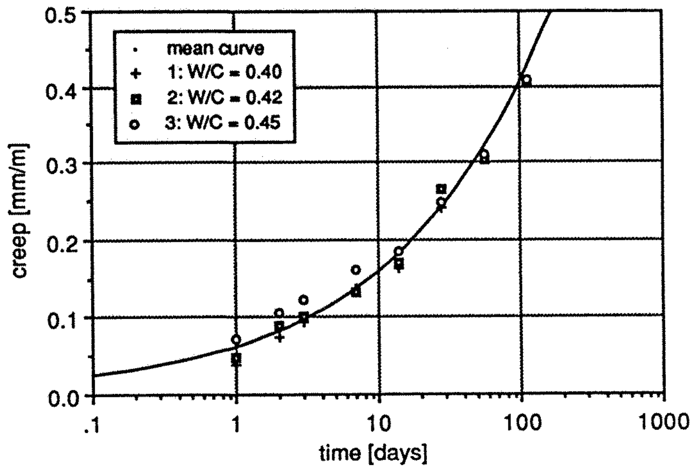

Figure 4: creep of the mortars.

Table 3: Adhesive strength of type 1 specimens

W/C	Tensile strength [MPa]	
	28 days	56 days
0.40	0.8	1.2
0.42	1.2	1.3
0.45	0.7	1.5

Table 4: adhesive strength of type 2 specimens

Mason	Tensile strength [MPa]			
	Facing S-O		Facing N - O	
	28 days	58 days	28 days	56 days
A	1.3	1.4	1.0	1.2
B	1.3	1.3	1.3	1.5

3.2 Non-destructive testing

Firstly, we must state that all the values and relations determined here are proper to the examined material. A new calibration of measurements is needed, if fundamental parameters of the material such as the type of cement, size distribution of the aggregates, C/A ratio are changed.
Moreover, the dynamic modulus of elasticity and the velocity of sound are related by an expression containing Poisson's ratio. We have assumed a value of $\upsilon = 0.27$, justified by the fact that dynamic measurements overestimate Poissons's ratio, compared with static methods.

$$f(\nu) = \frac{(1-\nu)}{(1+\nu)(1-2\nu)} \quad (17)$$

The measurements performed on normalized prisms have shown that there exists a linear relation between the velocity of sound and the W/C ratio, independent of time, as shown on figure 5. Conservation of linearity with the age of the samples results from the combined kinetics of cement hydration and pouzzolanic reactions associated with condensed silica fume, which conduct to the refinement of the porous structure in the mortar. The pore size distribution influences the velocity of sound in two ways:

- pores smaller than 1μm damp the acoustic pulses
- pores greater than 1 μm reduce the velocity, due to the acoustic coupling they induce.

The increase in compressive strength and velocity of sound being governed by the same mechanisms, we have fitted a master curve independent of time, which expresses the relation between two properties. This curve is calculated from the empirical relation between compressive strength and elastic modulus, and from the formula relying on the elastic modulus and the velocity of sound.

$$E_{stat} = k\sqrt[3]{f_{cc}} \quad (18)$$

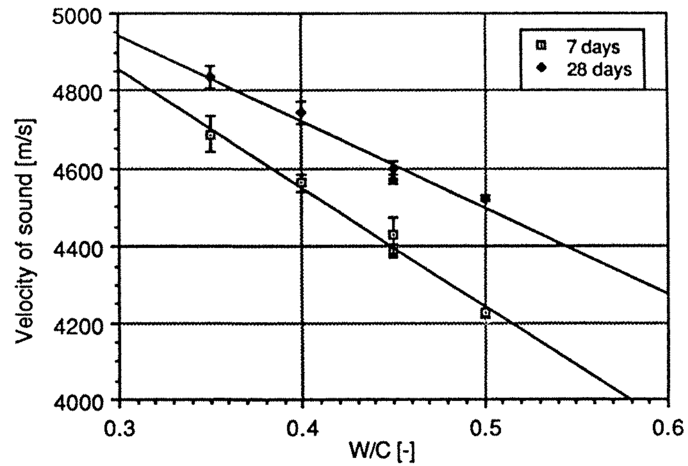

Figure 5:. Velocity of sound versus W/C ratio determined on normalized prisms.

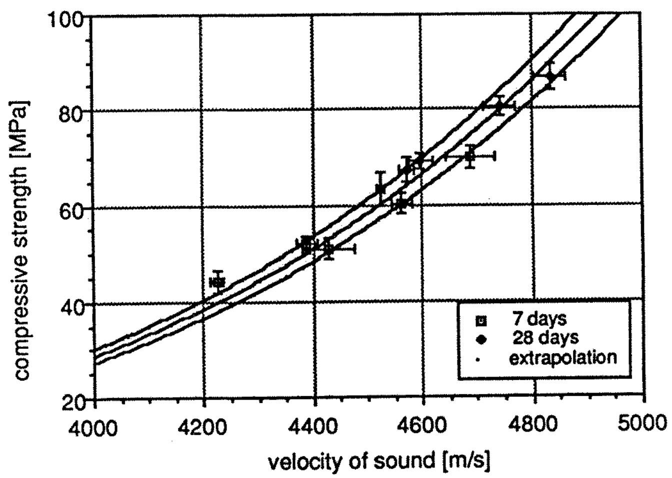

Figure 6: Compressive strength versus velocity of sound for normalized prisms. The experimental domain drawn on this figure is determined by assuming an error of 1,5% in the measurements of the velocity of sound.

The velocity of sound determined from the various parts of the experimental wall are represented in Figure 6. The velocities obtained for the screed are higher than those measured for the renderings, because the screed is more compact due to its horizontal application. The velocity of sound also depends on curing conditions, mainly on the pouzzolanic reactions: a t-test applied on the mean of sound velocities for both exposures reveals that the mean velocity of sound is higher for a N-E exposure than for a S-W, with a confidence of 97%.
The indirect measurements also permit a more accurate analysis of the structure, namely:

- the localisation of cracks in the mortar
- an information about the quality of the substrate

These two cases are shown in Figure 7. Decohesion at the interface mortar/concrete is equally detectable, with a combination of the previously treated cases.

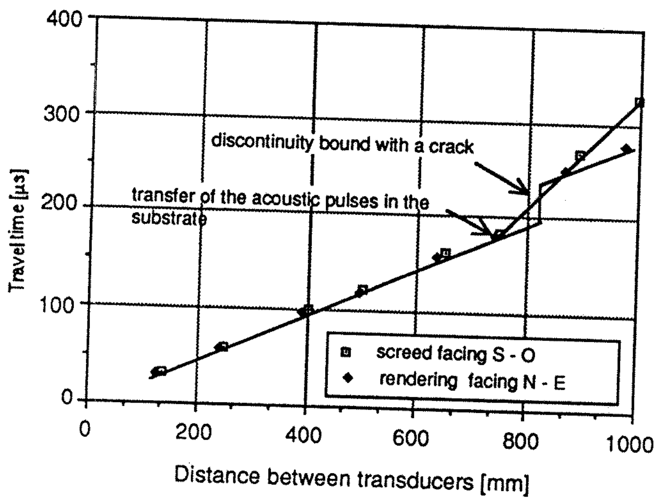

Figure 7: Possibility of measurements with ultrasonic testing. Detection of cracks - Quantifying the quality of the substrate concrete.

Finally, various restrictions have to be taken into account for in situ measurements:

- W/C ratio used for a handmade rendering is highly variable, the quantity of water varies on the application plane, moreover curing conditions also vary for a multilayer rendering.
- it is not possible to analyse a highly cracked material, where the spatial interaction of cracks does not allow the assumption of an homogeneous material.

One can see that measurements performed on the experimental wall may be superposed on the domain determined with normalized prisms (Figure 8). Following conclusions can be drawn.

- the vertical separation between the points corresponding to the experimental wall and the master curve results from the curing conditions of the material, where the superficial evaporation lowers W/C ratio locally. The case of the screed confirms this assumption, with bleeding during the first hours of curing.
- the horizontal separation is also bound with curing conditions, but in terms of long time curing: the development of the internal microstructure in the mortar is favorized by the N-E exposure (all points closer to the master curve).

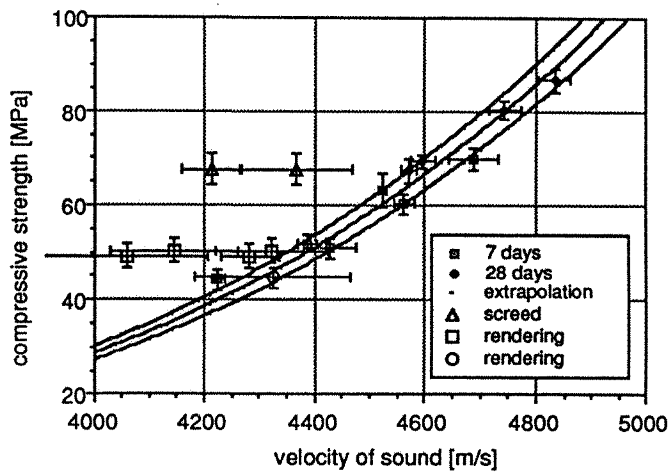

Figure 8: Compressive strength versus velocity of sound for normalised prisms and in situ measurements.

Thus the quality of a repair mortar can be measured by this method, particularly those containing condensed silica fume, which necessitate some weeks of curing at a high relative humidity to promote the pouzzolanic reactions.

3.3 Numerical simulation

The thermal history of the wall is shown in Figure 9. The greater variations are found at the surface (atmospheric conditions), whereas the damping of the fluctuations is due to thermal inertia of the materials.

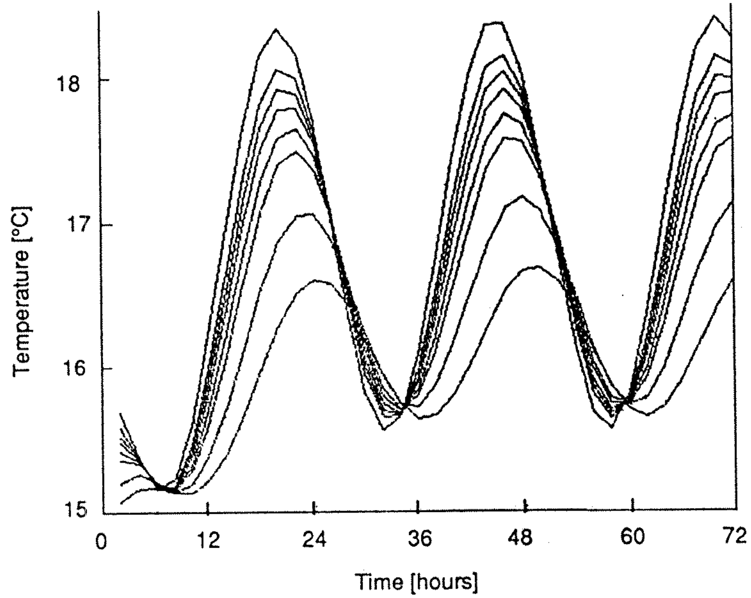

Figure 9: Thermal history of the wall

The state of the stresses in the x-y plane of the wall after 72 hours of curing is shown in Figure 10. ~~The state of the stresses in the x-y plane of the wall after 72 hours of curing is shown in Figure 10.~~ Solid lines represent tensile stresses, dashed lines represent compressive stresses. Surface is under compression, which allows to limit cracking during the early stages of curing. Compressive stresses at the mortar/concrete interface also allow to keep the risk of interfacial decohesion at a reasonable level. But tensile stresses higher than the intrinsic strength of the mortar develop under the surface, which could lead to cracking if curing conditions are inadequate. Figure 11 also shows the variations of the stresses σ_{zz} in plane strain conditions at various places in the wall. Maximum tensile stresses appear must under the surface of mortar, which is a great risk for the durability of the structure and therefore needs a powerful method for detection.

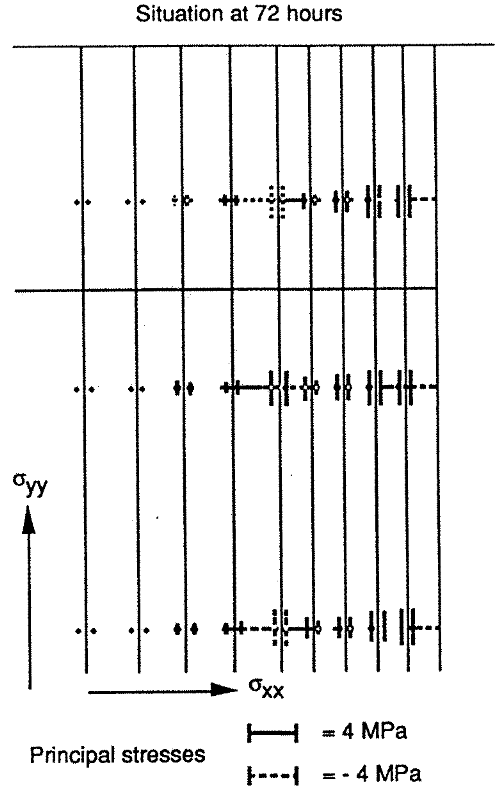

Figure 10:
State of the stresses in the x-y plane of the wall after 72 hours of curing

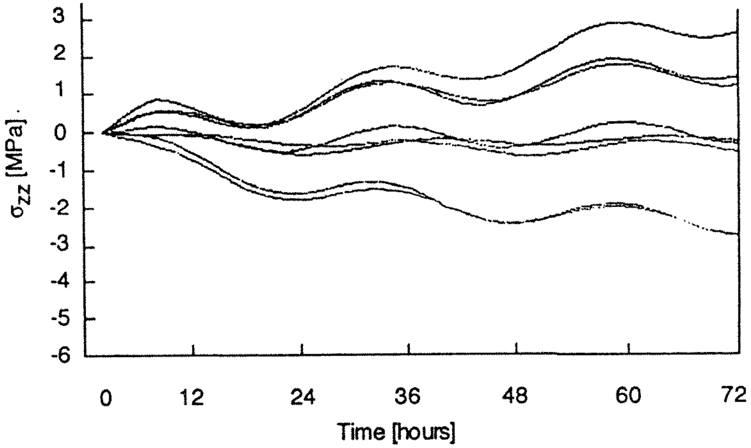

Figure 11: Variation of the stresses σ_{zz} in plane strain conditions at various places in the wall

4 Conclusion

The flexural and compressive strengths we have measured are very high. But in situ, they will generally be lower because of the curing conditions. Thus, the strengths will be nearer of the concrete substrate. The elastic modulus is lower to those than that of the concrete substrate which is generally an old concrete. This tends to lower the risks of cracking and decohesion.
The drying shrinkage of the mortars is lower than that generally found with concrete. Therefore the risk of decohesion is low.
The creep of the mortars is higher than that of standard concrete. This and the low shrinkage should promote a high durability of repair with this type of mortar.
The results of adhesive tensile strength measured on specimens kept outdoors are quite satisfactory. This confirms the above remarks on drying shrinkage and creep.
The ultrasonic method of testing permits a complete description of the extent of cracking in the repair material and its substrate.
Finally, numerical simulation has demonstrated that limiting cracks or decohesion requires particularly appropriate curing conditions.

References

[1] Nilsson L.O.: Hygroscopic Moisture in Concrete - Drying, Measurements and its related Material properties, Institute of Technology, Lund (1982).

[2] Hansen K.K.: Sorption Isotherms, a Catalogue, Technical Report 162/86, The Technical University of Danemark, Kobenhavn (1986)

[3] Bazant Z.P.; Najjar L.P.: Drying of Concrete as a nonlinear Problem Cem. Concr. Res., 1 (1971) 461-473.

[4] Roelfstra P.E.: A Numerical Approach to Investigate the Properties of Concrete - Numerical Concret, thése EPFL n° 788, Lausanne (1989).

[5] Alou F., Ferraris C. and Wittmann F.H.: Etude expérimentale du retrait du béton, Mater. Struct., **20** (1987) 323-333.

[6] Wittmann F.H., Bazant Z.P., Alou F. and Kim J.K.: Statistics of Shrinkage Tests Date, Cem. Concr. Aggr. **9** (1987) 129-153.

Acknowledgements

This research was supported in part by the Swiss Federal Office for Highways (OFR) which is gratefully acknowledged.

Werkstoffwissenschaften und Bausanierung, Teil 1

Materials Science and Restoration, Vol. 1

Tagungsbericht des dritten Internationalen Kolloquiums zum Thema Werkstoffwissenschaften und Bausanierung

Proceedings of the third International Colloquium on Materials Science and Restoration

Herausgegeben von Prof. Dr. F. H. Wittmann, ETH Zürich

Kontakt & Studium
Band 420

Herausgeber:
Prof. Dr.-Ing. Wilfried J. Bartz
Technische Akademie Esslingen
Weiterbildungszentrum
DI Elmar Wippler
expert verlag

expert verlag

1993